JGR Atmospheres

RESEARCH ARTICLE
10.1029/2019JD030650

Key Point:
- The MEP model is parsimonious and well suited to modeling surface energy budget in data-sparse permafrost environments

Correspondence to:
H. El Sharif,
helsharif@gatech.edu

Citation:
El Sharif, H., Zhou, W., Ivanov, V., Sheshukov, A., Mazepa, V., & Wang, J. (2019). Surface energy budgets of Arctic tundra during growing season. *Journal of Geophysical Research: Atmospheres*, *124*, 6999–7017. https://doi.org/10.1029/2019JD030650

Received 18 MAR 2019
Accepted 16 JUN 2019
Accepted article online 24 JUN 2019
Published online 9 JUL 2019

Surface Energy Budgets of Arctic Tundra During Growing Season

Husayn El Sharif[1], Wenbo Zhou[2], Valeriy Ivanov[2], Aleksey Sheshukov[3], Valeriy Mazepa[4], and Jingfeng Wang[1]

[1]School of Civil and Environmental Engineering, Georgia Institute of Technology, Atlanta, GA, USA, [2]Department of Civil and Environmental Engineering, University of Michigan, Ann Arbor, MI, USA, [3]Department of Biological and Agricultural Engineering, Kansas State University, Manhattan, KS, USA, [4]Institute of Plant and Animal Ecology, Ural Branch, Russian Academy of Sciences, Yekaterinburg, Russia

Abstract This study analyzed summer observations of diurnal and seasonal surface energy budgets across several monitoring sites within the Arctic tundra underlain by permafrost. In these areas, latent and sensible heat fluxes have comparable magnitudes, and ground heat flux enters the subsurface during short summer intervals of the growing period, leading to seasonal thaw. The maximum entropy production (MEP) model was tested as an input and parameter parsimonious model of surface heat fluxes for the simulation of energy budgets of these permafrost-underlain environments. Using net radiation, surface temperature, and a single parameter characterizing the thermal inertia of the heat exchanging surface, the MEP model estimates latent, sensible, and ground heat fluxes that agree closely with observations at five sites for which detailed flux data are available. The MEP potential evapotranspiration model reproduces estimates of the Penman-Monteith potential evapotranspiration model that requires at least five input meteorological variables (net radiation, ground heat flux, air temperature, air humidity, and wind speed) and empirical parameters of surface resistance. The potential and challenges of MEP model application in sparsely monitored areas of the Arctic are discussed, highlighting the need for accurate measurements and constraints of ground heat flux.

Plain Language Summary Growing season latent and sensible heat fluxes are nearly equal over the Arctic permafrost tundra regions. Persistent ground heat flux into the subsurface layer leads to seasonal thaw of the top permafrost layer. The maximum energy production model accurately estimates the latent, sensible, and ground heat flux of the surface energy budget of the Arctic permafrost regions.

1. Introduction

The Arctic has been warming since the early 1970s (Bekryaev et al., 2010), and the warming trend has been accelerating at unprecedented rates over the last decade (ACIA, 2004; Overpeck et al., 1997; Serreze et al., 2000). Chapin et al. (2005) reported warming rates for Arctic Alaska and western Canada increased from 0.15–0.17 (1961–1990) to 0.3–0.4 °C/decade since the 1990s. Surface air temperatures continue to warm at twice the global rate, and recent temperatures (since 2014) exceed all previous records since 1900 (Osborne et al., 2018). Warming amplification arguably results from strong positive land-atmosphere feedbacks as well as changes in the ocean-atmosphere heat exchange (Bonfils et al., 2012; Foley, 2005; Graversen & Wang, 2009; Jeong et al., 2012; Screen & Simmonds, 2010; Serreze et al., 2009; Serreze & Francis, 2006; Spielhagen et al., 2011; Swann et al., 2010). The changing climate in the region has already affected terrestrial ecosystems (Post et al., 2009), leading to increased "greening" of the Arctic (Bhatt et al., 2013; Forbes et al., 2010; Jia et al., 2003, 2009; Snyder, 2013) resulting from higher biomass production. Previous studies suggested that the response of vegetation in the Arctic ecosystems to the warming climate may represent a positive feedback through albedo as a primary driver of surface energy budget (e.g., Chapin et al., 2005; Essery & Pomeroy, 2004; Lee & Mahrt, 2004; Liston et al., 2002; Pomeroy et al., 1997, 2003, 2006; Sturm et al., 2001, 2005). Directly or indirectly, a greener Arctic will alter surface energy balance and subsurface thermal and moisture regimes (Hinzman et al., 2005; Loranty et al., 2016; Loranty et al., 2018; Loranty & Goetz, 2012; Osterkamp & Romanovsky, 1999). The increasing abundance and size of shrubs and trees alter the exchange of water and energy between the atmosphere, vegetation, and subsurface and hence have the potential to impact the fate of the permafrost with implications on biogeochemical feedbacks (Schuur et al., 2015).

Understanding the water and energy cycles in the Arctic is therefore urgently needed to predict the long-term impacts of the Arctic warming (Chapin et al., 2005). Yet quantification of the water and energy cycles in the Arctic is more challenging than in other regions due to the difficulties of continuous field observation as well as complex physics of seasonal changes associated with freeze-thaw cycle. Indeed, observational data for the Arctic are much less abundant compared to the other continental regions. The worldwide FLUXNET network that integrates micrometeorological observations (http://fluxnet.fluxdata.org/) has over 700 sites located below 65°N but fewer than 40 sites at higher latitudes (> 65°N; Falge et al., 2016). A number of research teams have carried out studies to characterize surface energy and water budgets in the Arctic, but direct measurements of water and energy fluxes are still sparse in space and time (Cristóbal et al., 2017). For example, Beringer et al. (2005) measured energy fluxes along a vegetation gradient and found an increase in growing season latent heat and sensible heating along a tussock tundra-spruce forest ecotone in Alaska. Soegaard et al. (2001) reported 2-year summer energy fluxes at Zackenberg (Greenland). A long-term record of energy fluxes focusing on summer seasons was reported later for the same site (Lund et al., 2014). Lund et al. (2017) later analyzed differences in energy budgets across tundra, snow, and ice surfaces at five sites in Greenland. Lloyd et al. (2001) studied surface energy fluxes during growing seasons at four sites across the European Arctic. Besides the scarcity of field data, the lack of energy budget closure remains to be a major issue in the analysis of energy budgets in the Arctic. Observed surface energy imbalance at some sites can reach 20% (Lund et al., 2017; Soegaard et al., 2001). This level of energy imbalance was commonly attributed to instrumental and model uncertainties, inaccurate estimation of storage terms, and the lack of representativeness due to the small scale of heat flux observations (Foken, 2008; Lund et al., 2014; Wilson et al., 2002).

With scarce field observations, water and heat fluxes have been simulated using process-based models for the Arctic regions (Boike, 2003; Cristóbal et al., 2017; Ueyama et al., 2014). These models of surface fluxes (Hamman et al., 2016; Qiu et al., 2018) do not always provide full characterization of energy budget (i.e., latent, sensible, and ground heat flux; Cristóbal et al., 2017), and the modeled fluxes often exhibit substantial uncertainties. These models also require in situ and/or remote sensing input data including meteorological forcing and land cover data that are often unavailable for remote Arctic regions (Ueyama et al., 2014).

It is well understood that energy exchange at the land-atmosphere interface in the Arctic is a crucial determinant of ecosystem function and the fate of belowground thermal state. The surface radiative budget as well as turbulent and conductive heat fluxes can be affected in magnitude and partition as the Arctic surface undergoes changes in response to the warming climate, potentially leading to feedback mechanisms that will enhance or dampen the induced changes. Further studies are necessary to characterize water and energy cycle in the Arctic, especially for permafrost regions. As in situ observations of energy fluxes in the Arctic are costly, there is a need for developing efficient and robust modeling tools. The maximum entropy production (MEP) model of surface heat fluxes (Wang et al., 2014; Wang & Bras, 2011) is a novel approach that uses fewer input data and model parameters than does the classical bulk transfer models (e.g., Arya, 1988) and Penman-Monteith (P-M) model of evapotranspiration (e.g., Brutsaert, 1982). In addition to input data parsimony, the MEP model has more advantages compared to other surface energy budget models to be more suitable for permafrost regions. The MEP model closes the surface energy budget at all space-time scales. The MEP model does not require the data of wind speed, surface roughness, and vertical gradients of temperature and vapor pressure, which are subject to high uncertainty and difficult to measure in the harsh Arctic environments. The MEP model holds for full range of soil moisture and snow/ice surfaces. The MEP model has been shown to outperform other existing models (Hajji et al., 2018; Huang & Wang, 2016; Shanafield et al., 2015; Wang et al., 2014; Wang et al., 2017; Wang & Bras, 2011; Xu et al., 2019; Yang & Wang, 2014). In this study, the MEP model is utilized with two objectives: (i) to evaluate the surface energy budgets across a range of vegetation covers in the Arctic permafrost areas and (ii) to confirm the MEP model as an efficient and robust model of potential evapotranspiration (PET).

2. Data and Method

2.1. Data

The global FLUXNET network (http://fluxnet.fluxdata.org/; Baldocchi et al., 2001), the AmeriFlux network (http://ameriflux.lbl.gov/), and the Arctic Observatory Network (http://aon.iab.uaf.edu/) provide

Table 1
Information on the Study Sites

Site	Latitude/longitude/ elevation (m a.s.l.)	Mean annual (summer) air temperature (°C)	Mean annual (summer) precipitation (mm)	Analysis period	Land surface condition	Data source
Ivotuk, AK, USA	68.49/−155.75/568	−8.28 (~12)[b]	304 (210)	6/15–8/31 2004–2007	Permanent wetland, tussock sedge, dwarf shrub, moss tundra	FLUXNET DOI: https://doi.org/10.18140/FLX/1440073
Kuparuk River, AK, USA	70.28/−148.88/5	−13.6 (5.5)	124 (80)	6/15–8/31 1994	Permanent wetland, tussock tundra	AmeriFlux DOI: https://doi.org/10.17190/AMF/1246108
Imnavait Creek: Ridge Flux Tower, AK, USA	68.61/−149.30/951	−7.4 (9.4)[c]	318 (~230)	6/1–8/31 2017	Tussock and heath tundra	Arctic Observatory Network, http://aon.iab.uaf.edu/
Imnavait Creek: Tussock Flux Tower, AK, USA	68.61/−149.30/918	−7.4 (9.4)[c]	318 (~230)	6/1/–8/31 2017	Tussock tundra	Arctic Observatory Network, http://aon.iab.uaf.edu/
Vorkuta, Komi Republic, Russia	67.05/62.95/100	−5.8 (9.4)	505 (172)	6/15–8/31 2008	Heath tundra, closed shrubland	FLUXNET DOI: https://doi.org/10.18140/FLX/1440245
Polar Urals, Yamal-Nenets Autonomous District, Russia[a]	66.8163/65.5723 ("tundra") 66.8526/65.6475 ("trees")	−6.7 (9.6)	500–600 (276)	6/26-8/25 2015–2017	"Tundra" site: moss-lichen and heath tundra with rock outcrops "Trees": Siberian larch, dwarf shrubs, heath tundra	NSF Arctic Data Center, http://arcticdata.io/ DOI: https://doi.org/10.18739/A2C824D80

[a]No eddy-covariance flux data available. [b]Mean July maximum daily temperature. [c]Mean July temperature.

observations of latent, sensible, and ground heat fluxes and other hydrometeorological variables that are used for analyzing the surface energy budgets and testing the MEP models. Half-hourly flux data and/or other hydrometeorological variables are publicly available for six sites in areas underlain by the permafrost located in the United States and Russia. Relevant site specifics, land surface conditions, and sources of data are provided in Table 1, and details of instrumentation are discussed below. No direct observations of surface fluxes were available at the Urals site.

Ivotuk, AK, USA: The Ivotuk tundra site is located on the North Slope of the Brooks Mountain Range. Vegetation types at the site include moist tundra and shrub tundra. Mean annual temperature and precipitation are −8.28 °C and 304 mm, respectively. Mean July maximum daily temperature is ~12 °C, and mean summertime precipitation is 210 mm (Parazoo et al., 2018; Riedel et al., 2005). Half-hourly data from years 2004–2007 were made available through the FLUXNET network (Zona & Oechel, 2004). Eddy-covariance instrumentation included a high-frequency (10 Hz) open-path infrared gas analyzer (IRGA, LI-7500, LI-COR Inc., Lincoln, NE, USA) and ultrasonic anemometer (R3, Gill Instruments) installed at 3 m above ground. Net radiation was measured using a four-channel CNR1 net radiometer (Kipp & Zonen, Delft, Netherlands). Ground heat flux was measured with six ground heat flux plates (HFT-1, REBS) installed at 5-cm depth within 20 m of the flux tower location. For this and all sites of this study, the widely adopted calorimetric method was used to derive ground heat flux from the soil heat flux measured at 5-cm depth and soil temperature measurements (Campbell Scientific, 2016; Fuchs & Tanner, 1968; Sauer & Horton, 2005; Oncley et al., 2007; Evett et al., 2012; Eshonkulov et al., 2019). Air temperature and relative humidity were measured by an HMP45C-L sensor (Vaisala Inc., Helsinki, Finland; Laskowski, 2010).

Kuparuk, AK, USA: The site is located in the arctic coastal plain of the North Slope of Alaska 10 km south of the Arctic Ocean and is characteristic of wet herbaceous tundra. Mean annual temperature and precipitation are −13.6 °C and 124 mm, respectively. Mean summer temperature and precipitation are 5.5 °C and 80 mm, respectively. An eddy-covariance system consisted of a 3-D sonic anemometer (Model SWS-21 1/3K, Applied Technologies Inc., Boulder, CO, USA) and closed-path (Model LI-6262, LI-COR Inc., Lincoln, NE, USA) and open-path infrared gas analyzers designed by the National Oceanic and Atmospheric Administration, Atmospheric Turbulence and Diffusion Division (Auble & Meyers, 1992). Measurements were taken at 10-Hz frequency with fluxes computed as 30-min averages. Air temperature at 2-m height was measured with a ventilated psychrometer. Net radiation was measured at 1-m height with a net radiometer (Model Q-6, REBS, Campbell Scientific, Inc., Seattle, WA, USA). Ground heat flux was measured with two heat flux plates (Model HFT-1, REBS, Campbell Scientific, Inc.) buried at 1- to 2-cm depth. Data collected during the summer of 1994 were made available through the AmeriFlux Network (Oechel, 1994; Oechel et al., 1993; Vourlitis & Oechel, 1997; Walker & Acevedo, 1987).

Tussock and Ridge Flux Tower sites, Imnavait Creek, AK, USA: Located at the headwaters of the Kuparuk River Basin in the northern foothills of the Brooks Range, AK, the Tussock Flux tower was installed at a moist tundra dominated by tussock and dwarf shrubs, whereas the Ridge site was at the dry watershed divide area characterized by heath tundra system. Mean annual temperature was −7.4 °C, and mean annual precipitation was 318 mm. July mean temperature is 9.4 °C, and mean summertime precipitation is about 230 mm. The eddy-covariance systems at both sites were installed at 2.5- to 3-m height and consisted of a 3-D sonic anemometer (CSAT-3; Campbell Scientific Instruments, Logan, UT, USA) and an open-path infrared gas analyzer (LI-7500 IRGA; LI-COR, Lincoln, NE) with 10-Hz sampling frequency. Air temperature and relative humidity were measured at 2-m height (HMP45C, Vaisala Inc., Helsinki, Finland), and ground heat flux was measured with three heat flux plates (HFP01-SC, Hukseflux, Delft, Netherlands) installed at 5-cm depth. A net radiometer (single-channel NR-LITE radiometer, Kipp & Zonen, Delft, Netherlands) was installed at 2-m height. Surface and 2.5-cm soil temperature were measured by an averaging soil thermocouple probe (Campbell Scientific Instruments; Schramm et al., 2007; Euskirchen et al., 2012). Data for the summer of 2017 were provided through the Arctic Observatory Network.

Vorkuta, Komi Republic, Russia: The Vorkuta site is located near the village of Seida in northwestern Russia. Land cover includes tundra heath, peat plateau, and permafrost peatland. Mean annual temperature was −5.8 °C, and mean precipitation was 505 mm (Repo et al., 2009). Mean summertime temperature and precipitation are 9.4 °C and 172 mm, respectively. Data collected during the summer of 2008 were provided by the FLUXNET network (Friborg et al., 2008; Heikkinen et al., 2004).

Polar Urals, Yamal-Nenets Autonomous District, Russia: Two sites ("tundra" and "trees") on the eastern slope of the Polar Urals range represent a natural gradient of land surface conditions in the tundra-forest transitional zone underlain by the continuous permafrost. There has been a significant expansion of open and closed larch forests to moss-lichen and heath tundra areas over the past 50–60 years, with horizontal displacement rates of 32–58 m/decade and altitudinal rates of 3–4 m/decade (Devi et al., 2008; Mazepa, 2005; Shiyatov et al., 2005; Shiyatov et al., 2007). The mean annual air temperature at Salekhard (55 km southeast of the site location) is −6.7 °C. The mean annual precipitation was 500–600 mm, with ~50% as snow and sleet. The mean frost-free period is 94 days with the growing season from mid-June to mid-August. According to reanalysis data from Modern-Era Retrospective Analysis for Research and Applications, version 2 (MERRA-2), summer mean temperature is 9.6 °C, and summer precipitation is about 276 mm (Gelaro et al., 2017; Global Modeling and Assimilation Office, 2015a; Global Modeling and Assimilation Office, 2015b). The tundra site (Table 1) is located near the upper east-side corner of a continuous altitudinal transect (Mazepa, 2005) in the vicinity of Tchernaya Mountain. Moss-lichen tundra with rock outcrops (10–25%) and deciduous shrub communities (up to 0.5-m-high dwarf birch, creeping willow, and northern bilberry) are the dominant land covers. The trees site is mountain heath tundra encroached by the Siberian larch in the past 30 years, with current surface canopy cover 20–40%, 3- to 4-m average height, and individual trees reaching 8 m. Both sites have identical observational instrumentation. Air temperature and relative humidity were measured at 2-m height (CS215 Temperature and Relative Humidity probe; Campbell Scientific Instruments, Logan, UT, USA). Net radiation and downwelling/upwelling shortwave radiation (single-channel NR-LITE2 net radiometer and CMP3 pyranometer; Kipp & Zonen, Delft, Netherlands) were measured at 2.5 (tundra) and 5 m (trees). Surface temperature was measured using Apogee Infrared radiometer (SI-111; Apogee Instruments, Inc., Logan, UT, USA). Sap flow was measured using the modified heat-dissipation method (Granier, 1987) in emergent larch trees at 20-min resolution. To translate the measured temperature differences between the heated and reference needles (measured in volts) into a "proxy" for sap flow velocity, V, we use $V = \alpha \left(\frac{dT_M - dT}{dT}\right)^{\beta}$, where dT_M is the baseline or zero flow temperature difference, dT is the temperature difference of flowing sap, and α and β are fitting coefficients that are assumed to be unity. The value of dT_M is chosen as the maximum voltage measured on nights with small vapor pressure deficit and calm conditions and assumed to be representative for the entire growing season. The Poral Urals data set is publicly available at the National Science Foundation (NSF) Arctic Data Center (Mazepa et al., 2019).

2.2. Methods

2.2.1. The MEP Model of Surface Energy Budget

Direct measurements of surface heat fluxes using eddy-covariance systems are only available for a small fraction of monitoring sites in the Arctic region. Suitable models are needed for the estimation of heat fluxes over large areas using limited field observations (when available) or remote sensing data. Traditional bulk flux formula require data on temperature and humidity gradient, wind speed, and surface roughness not observable from remote sensing platforms. A novel method known as the MEP model was developed by Wang and Bras (2011) and Wang et al. (2014) to overcome the difficulties of bulk flux models for data-sparse regions.

The theoretical foundation of the MEP model is the modern nonequilibrium thermodynamics. The MEP principle (Dewar, 2005; Dewar et al., 2014) is a special case of the well-established principle of maximum entropy (MaxEnt; Jaynes & Bretthorst, 2003) originally proposed as an application of information theory in statistical mechanics (Jaynes, 1957). Since then, MaxEnt has been applied widely in science and engineering (e.g., Kapur, 1989). The more recent MEP theory has also been increasingly applied (Kleidon & Lorenz, 2005) in land surface hydrology (Kleidon & Schymanski, 2008) for modeling dynamics of bio-ecological systems (Juretić & Županović, 2003; Kleidon et al., 2010; Kleidon & Fraedrich, 2006; Shipley, 2010). Details of the application of the MEP theory to the formulation of surface heat fluxes are described in Wang and Bras (2009, 2011). A unique feature of the MEP model is that it provides a simultaneous solution of latent, sensible, and ground heat fluxes without using temperature and humidity gradients, wind speed, and roughness data. A key parameter of the MEP model is surface soil thermal inertia. The MEP model of latent E, sensible H, and ground G heat flux over land surfaces has the following analytical expression (Wang & Bras, 2011):

$$
\begin{aligned}
&E + H + G = R_{\mathrm{n}} \\
&E = B(\sigma)H \\
&G = \frac{B(\sigma)}{\sigma}\frac{I_{\mathrm{s}}}{I_0}H|H|^{-\frac{1}{6}} \\
&B(\sigma) = 6\left(\sqrt{1 + \frac{11}{36}\sigma} - 1\right), \sigma \equiv \frac{\lambda^2}{c_{\mathrm{p}}R_{\mathrm{v}}}\frac{q_{\mathrm{s}}}{T_{\mathrm{s}}^2}
\end{aligned}
\tag{1}
$$

where R_{n} is net radiation, I_{s} the (surface) soil thermal inertia,I_0 the "apparent thermal inertia of the air" (Appendix A), T_{s} surface temperature (K), q_{s} surface specific humidity (kg/kg), and σ the proportional coefficient between the thermal inertia of latent and sensible heat flux (Wang & Bras, 2011). The dimensionless σ characterizes the relative role of water and thermal state of the evaporating surface in the phase change of liquid water (see Appendix A for more details). Radiation fluxes toward the land surface are defined as positive. The signs of E, H, and G are taken as opposite to that of radiation fluxes. Specific humidity q_{s} ranges from 0 to saturation level at surface temperature and implicitly depends on soil moisture. The MEP solution of E, H, and G is obtained from the nonlinear algebraic equation as in the system of equation (1) using the data on R_{n},T_{s},and q_{s}. B is the reciprocal Bowen ratio as a function of temperature- and humidity-dependent σ that characterizes the relative roles of surface thermal and moisture condition in surface energy budget. The MEP model for snow (and water) surfaces has a similar formulation to that in equation (1) (see Appendix B).

The land cover conditions of areas in the Arctic exhibit a pronounced seasonal cycle from partial-to-full canopy coverage during the growing season to full snowpack cover during winter. In this context, the MEP model in equation (1) has been shown to be more advantageous than the traditional bulk flux models, due to its parsimony in model input and parameters. In particular, the model does not need seasonally variable surface roughness and constantly varying wind speed, which are difficult to obtain for data-poor Arctic regions of high surface heterogeneity.

The thermal inertia of surface material $I_{\mathrm{s}} = \sqrt{k\rho c_{\mathrm{h}}}$ (with the unit thermal inertia unit, or tiu, J·m^{-2}·K^{-1}·s$^{-1/2}$; Putzig, 2006) depends on the thermal properties of surface materials such as mineral soil, rock outcrop, organic matter, or snow, where k is thermal conductivity (W·m^{-1}·K^{-1}), ρ is material density (kg/m^3), and c_{h} is specific heat capacity (J·kg^{-1}·K^{-1}). Theoretically, an "effective" thermal inertia of a heterogeneous evaporating surface may be defined as an area-weighted average of thermal inertia for individual land covers (e.g., rocks, soil, organic matter, and snow). In practice, however, accurate estimation of thermal inertia for a heterogeneous surface is challenging, especially in the presence of surface peat mat and soil organic

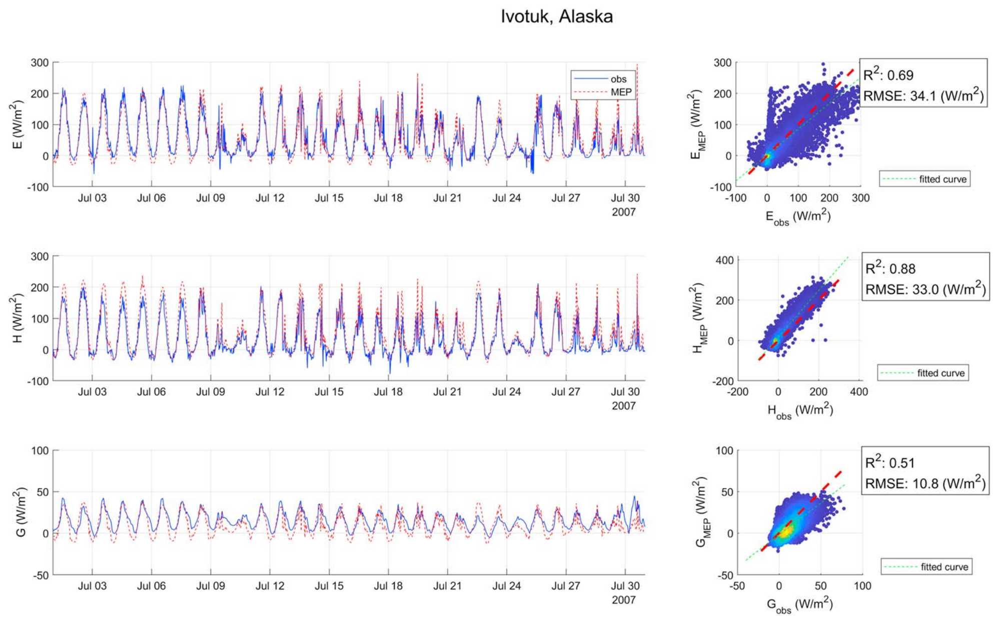

Figure 1. Half-hourly latent E, sensible H, and ground heat G flux estimated using the maximum entropy production model ("MEP") as in equation (1) versus half-hourly field observations ("obs") at Ivotuk, AK, USA. The left subplots show flux time series for July 2007. The scatterplots in the right column include all data points for the period of 5 June to 31 August 2004–2007. RMSE = root mean square error.

matter, which are common in the Arctic regions. An inverse approach is used in this study for estimating growing season thermal inertia of the surface layer at the case study sites. Surface thermal inertia is determined by minimizing the root mean square error (RMSE) between the MEP-modeled and in situ measured (half-hourly) ground heat flux. Appendix C provides further information on the estimation of I_s. Table A1 lists the obtained thermal inertia for growing season surface at all study sites.

2.2.2. The MEP Model of PET

Penman (PM) and P-M model (Monteith, 1965) are the commonly used models of PET using hydrometeorological data. In this study, PET is modeled using the method adopted by the Food and Agriculture Organization of the United Nations Paper No. 56 P-M equation (Allen et al., 1998). Refer to Appendix D for further details on model parameterization.

The MEP model as in equation (1) can be also seen as a PET model with fewer input variables. Since PET is defined as hypothetical evaporation over wet (or saturated) soil or canopy without water stress under the same meteorological conditions (e.g., net radiation and air temperature), the MEP model is a natural alternative PET model, if q_s in equation (1) is replaced by the saturation specific humidity at surface temperature, as seen in equation (B2). This new PET model will be referred to hereafter as the "MEP PET model."

There are notable advantages of the MEP PET model compared to the PM/P-M PET model. First, the MEP PET model uses only two input variables: net radiation and surface temperature. Second, it provides ground heat flux associated with PET as an output, while the PM/P-M PET models require ground heat flux as an input. These advantages make the MEP PET model better suitable for the study of energy balances in the Arctic, where field observations are sparse due to the difficulty of field measurements of ground heat flux and wind speed, among other hydrometeorological variables.

3. Surface Energy Budgets

Five of the six flux sites (Table 1) have half-hourly eddy-covariance data on latent and sensible heat fluxes that are used for the assessment of surface energy budgets and the evaluation of surface heat fluxes using the MEP model. Due to the harsh environmental conditions, field observations were mostly collected during summers. In this study, we use the data collected during the months of mid-June through end of August to analyze the energy budgets during growing seasons.

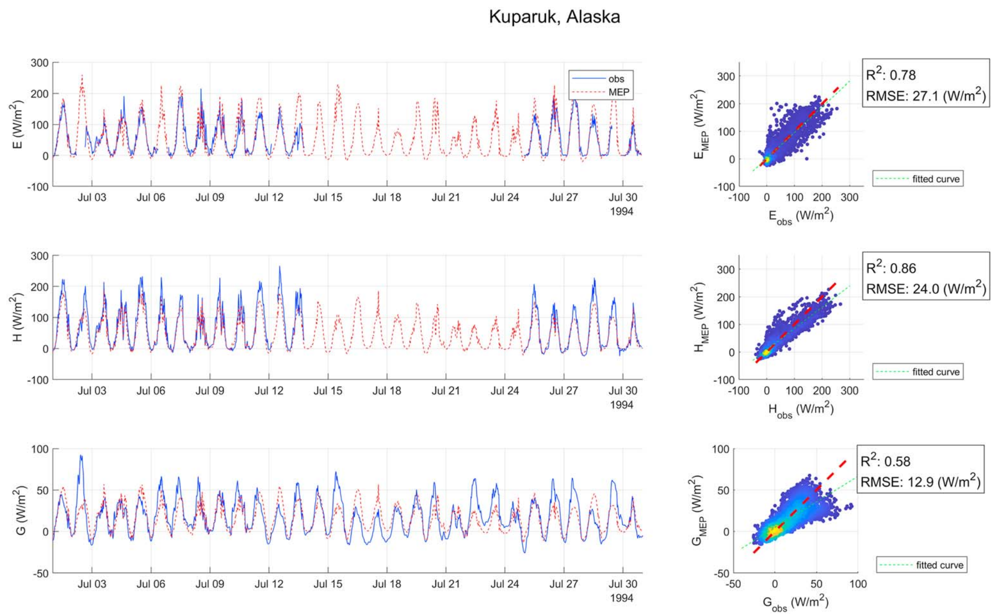

Figure 2. The same as Figure 1 for Kuparuk River, AK, USA. The left column shows plots of MEP-estimated versus observed half-hourly fluxes for July 1994. The scatterplots on the right include all data points for the period of 15 June to 31 August 1994.

The five flux sites are located within a narrow belt of 67–70°N latitude with the diurnal peak of solar radiation ~600–700 W/m^2 and net radiation ~400 W/m^2 with albedo of 16% consistent at all sites where incoming and reflected solar radiation were measured (data not shown). Figures 1–5 show the modeled versus observed surface energy budgets at those five sites. Latent and sensible heat fluxes are nearly equal with a diurnal peak around 200 W/m^2. With almost 24 hr of light in the Arctic Circle during July, this level of latent heat flux corresponds to daily evapotranspiration of ~2–3 mm, consistent with magnitudes representative of the lower-latitude regions.

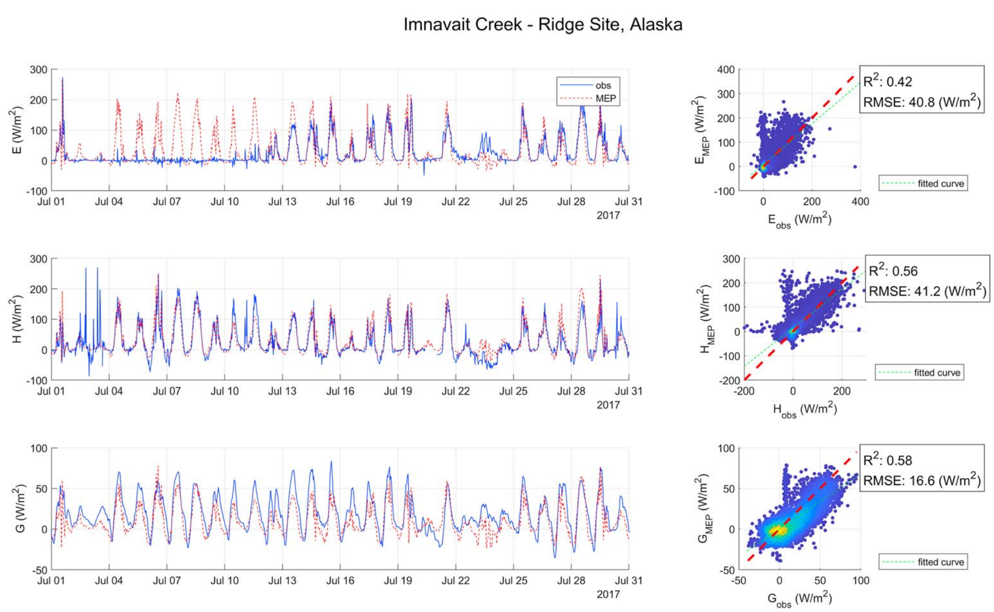

Figure 3. The same as Figure 1 for Ridge Flux Tower site, Imnavait Creek, AK, USA. The left column shows plots of MEP-estimated versus half-hourly observed fluxes for July 2017. The scatterplots on the right include all data points for the period of 1 June to 31 August 2017.

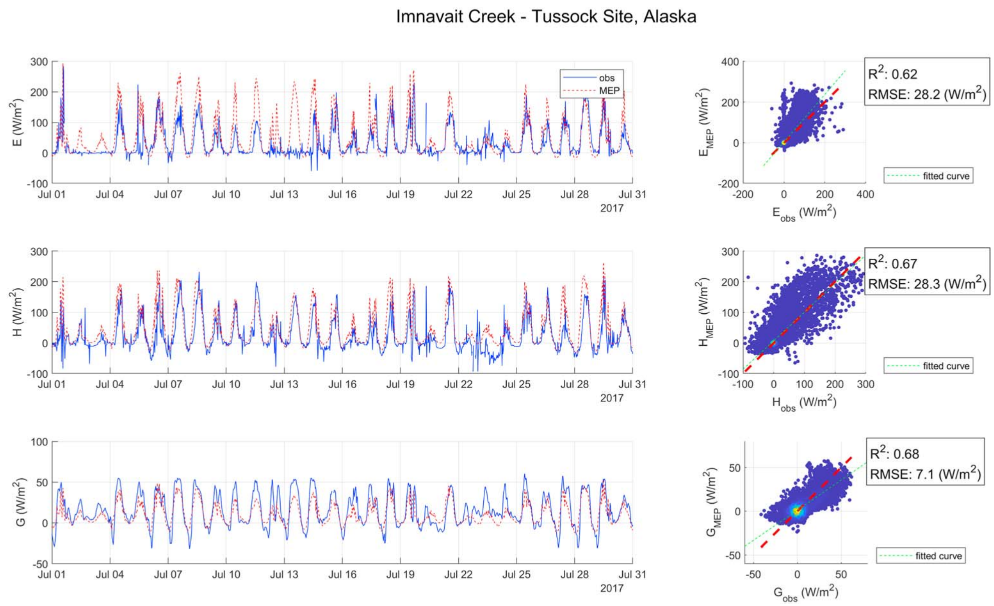

Figure 4. The same as Figure 1 for Tussock Flux Tower site, Imnavait Creek, AK, USA. The left column shows plots of MEP-estimated versus half-hourly observed fluxes for July 2017. The scatterplots on the right include all data points for the period of 1 June to 31 August 2017.

Contrary to the lower-latitude regions, ground heat flux plays an essential role in the Arctic system (Loranty et al., 2018). In particular, ground heat flux has the dominant impact on the permafrost dynamics by changing soil thermal and water regimes. Half-hourly ground heat fluxes at the five sites are mostly positive with the diurnal peaks of ~30–60 W/m^2, indicating that thermal energy flows into the soil layer, providing the heat source for ice thaw and the development of the seasonal active layer. Ground heat flux is a key boundary condition for modeling the thermodynamics of the active layer (although this problem is beyond the scope of this study). The relatively low magnitudes of ground heat

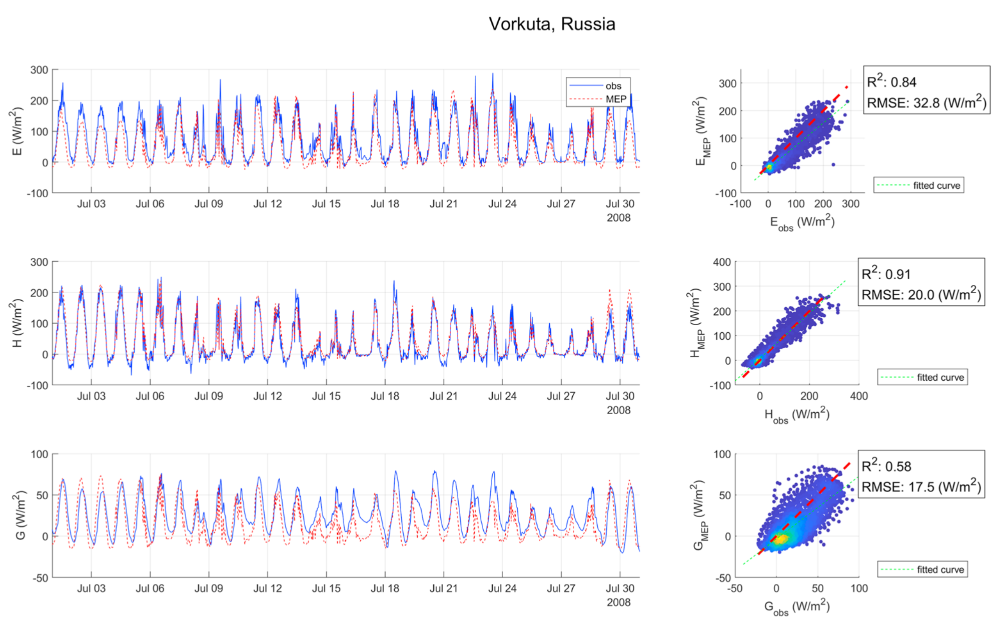

Figure 5. The same as Figure 1 for Vorkuta, Russia. The left column shows plots of MEP-estimated versus half-hourly observed fluxes for July 2008. The scatterplots on the right include all data points for the period of 15 June to 31 August 2008.

Table 2
Statistics of MEP-Modeled Versus Observed Latent, Sensible, and Ground Heat Fluxes at the Hourly Scale for the Five Study Sites

	Latent heat flux/sensible heat flux/ground heat flux						
Site name	RMSE (W/m^2)	NRMSE (%)	Correlation	Mean bias (W/m^2)	Mean absolute error (W/m^2)	Regression slope	Regression intercept (W/m^2)
Imnavait Creek Ridge	40.83/41.23/16.55	101/75/69	0.65/0.75/0.76	3.37/9.43/−5.12	24.62/24.74/12.92	0.85/0.79/0.67	7.73/14.68/0.15
Imnavait Creek Tussock	28.21/28.32/7.12	94/67/57	0.79/0.82/0.82	5.63/6.71/−0.14	10.39/11.88/3.21	1.17/0.93/0.69	3.79/7.48/1.13
Ivotuk	34.07/32.98/10.75	59/59/88	0.83/0.94/0.72	−6.24/21.43/−5.06	23.50/25.31/8.72	0.83/1.15/0.76	1.67/17.45/−1.87
Kuparuk Basin	27.15/23.98/12.90	50/39/65	0.88/0.93/0.76	−1.08/-2.42/−1.13	19.07/17.01/9.63	0.93/0.77/0.62	2.07/7.81/4.63
Vorkuta, Russia	32.83/20.03/17.45	52/31/79	0.92/0.95/0.76	−21.66/4.77/−8.70	24.79/14.18/14.08	0.83/0.91/0.76	−11.87/7.81/−3.47

Note. NRMSE uses the standard deviation of observation data as a normalization constant. MEmaximum entropy production; RMSE = root mean square error; NRMSE = normalized root mean square error.

flux (on the order of 50-W/m^2 diurnal peak) and the high level of subsurface saturation in the Arctic may be responsible for the relatively shallow active layer (~0.5–1 m; e.g., Yi et al., 2018) in this latitudinal band of the Arctic region.

Figures 1–5 show a good agreement between the MEP-modeled surface heat fluxes and the observations for all sites. Using only three input variables, that is, net radiation, surface temperature (or air temperature as a surrogate, when surface measurements are unavailable), and humidity, the MEP model provides the complete surface energy budget partition. The performance of the MEP model is demonstrated through scatterplots in the right-hand side panels of Figures 1–5. The corresponding performance statistics are reported in Table 2. In particular, the MEP latent heat flux is in close agreement with observations with no obvious biases. The MEP ground heat flux shows a slight phase shift relative to the observation, which is likely due to the fact that soil heat flux sensors are located at a certain depth below the surface: Even using the calorimetric method to take the effect of soil heat storage into account (Campbell Scientific, 2016), the biases in the corrected ground heat flux data cannot be completely removed. The MEP model accurately captures the diurnal variations of ground heat flux without spurious phase shifts.

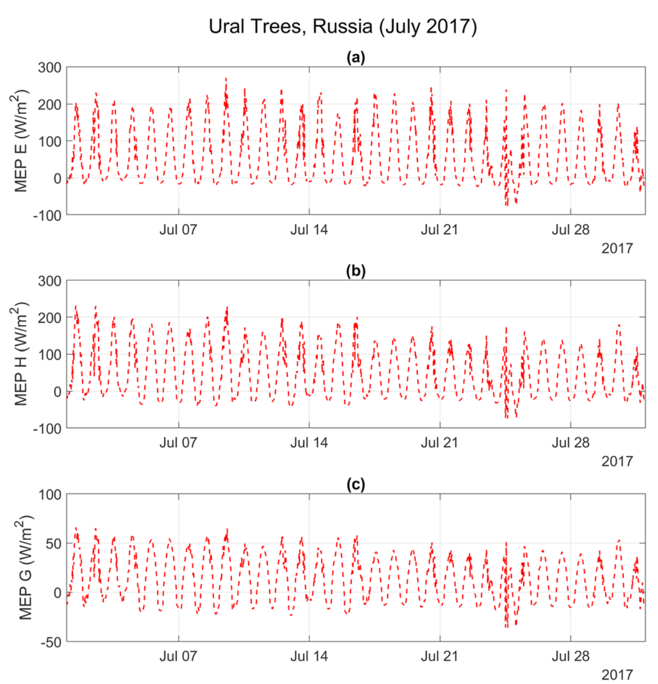

Figure 6. The half-hourly surface fluxes estimated using the maximum entropy production (MEP) model as in equation (1) for the “trees” site, Polar Urals, Russia, for July 2017. No direct heat flux measurements are available for this site.

Figure 6 shows the MEP surface heat fluxes computed using the observed net radiation, air temperature, and specific humidity (as the surrogates of surface temperature and specific humidity, not shown) at the trees site in Polar Urals, Russia (Table 1). Although no eddy-covariance or conductive flux observations are available for this site, the MEP surface energy budgets are consistent with those at the other sites with similar net radiation and surface temperature/humidity, that is, comparable latent and sensible heat flux with diurnal peak of ~ 200 W/m^2, Bowen ratio ~0.8–0.9, and ground heat flux with a diurnal peak ~50 W/m^2. The sap flow data shown in Figure 7a suggests that the MEP E is consistent with sap flow as a surrogate of E. Although the comparison is qualitative without converting the sap flow signals to E, the close correlation between them indirectly validates the MEP E estimates.

Overall, the MEP model estimates that on average 11% to 19 % of July daytime net radiation is partitioned into ground heat flux, 41% to 45% into latent heat flux, and 39% to 47% into sensible heat flux. Even though the MEP model is not overly sensitive to the surface thermal inertia, it is nevertheless vital to have a reasonable estimate (e.g., within an uncertainty of ~200 tiu, according to the analysis in Figure C1) to accurately simulate the surface energy budgets. Since the measurement errors of conductive ground heat flux are smaller than those of turbulent latent and sensible heat flux (Twine et al., 2000), the surface thermal inertia estimated by minimizing the differences between the MEP-modeled and observed ground heat flux (i.e., as was done in this study) is expected to be most appropriate.

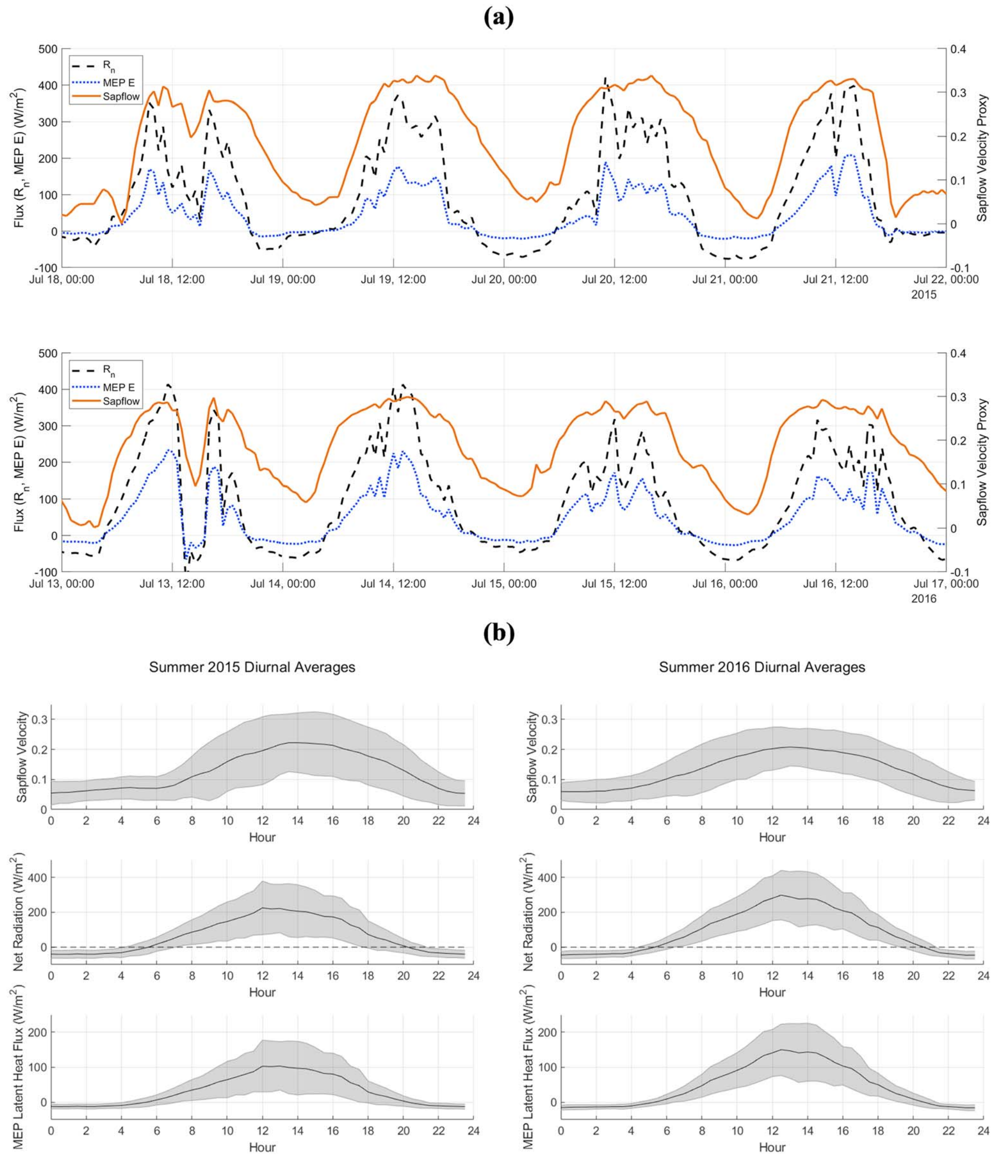

Figure 7. (a) Time series of net radiation, maximum entropy production (MEP) *E*, and sap flow velocity proxy at the Urals "trees" site at the half-hourly time step during select days of the summers 2015 and 2016. (b) Average (solid line) and standard deviation (shaded region) of diurnal cycles of adjusted sap flow signal, net radiation, and MEP *E* for the analysis periods of 2015 and 2016.

The effect of this parameter on the MEP-modeled energy budgets is further understood, when thermal inertia is estimated by minimizing the (square) differences between the modeled and observed turbulent heat fluxes. As mentioned previously, measurement errors of turbulent fluxes typically exceed those of ground heat flux, and the net available energy (i.e., $H + E$) estimated using the eddy-covariance technique tends to underestimate energy as compared to what is obtained from independently measured net radiation and ground heat flux (i.e., R_n – G). At the Imnavait Creek Tussock and Ridge sites, for example, when the thermal inertia parameter of the MEP model is calibrated using the biased turbulent fluxes, the "optimal" surface thermal inertia is estimated to be in the range of 800–1,200 tiu, instead of 200–400 tiu obtained using minimization of errors with respect to G. Such an overestimation of thermal inertia results in overestimation of MEP ground heat flux that far exceeds measurement errors, with diurnal peaks ~180 W/m^2 in July, instead of observed 30–60 W/m^2. On the other hand, when the net measured available energy from turbulent fluxes does not exhibit biases with respect to $R_n - G$, for example, at the Kuparuk site, neither the estimated

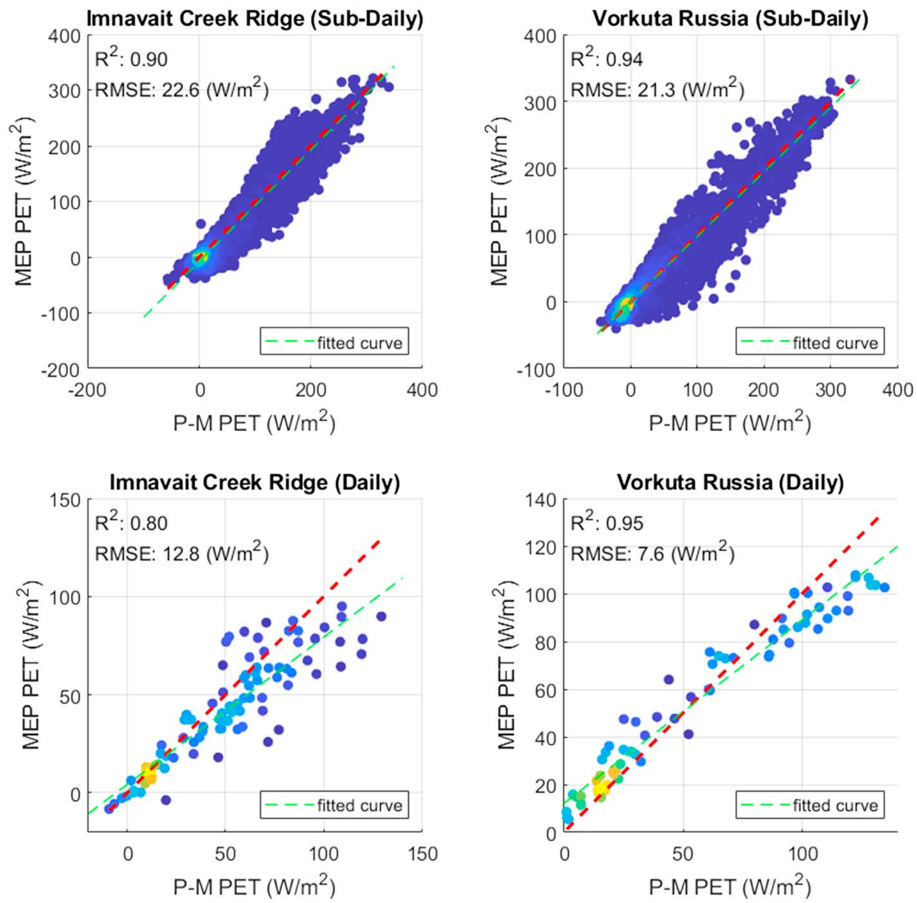

Figure 8. Penman-Monteith (P-M) versus maximum entropy production (MEP) potential evapotranspiration (PET) estimates at the (top) half-hourly scale and (bottom) daily scale for the Imnavait Creek Ridge and Vorkuta sites. RMSE = root mean square error.

surface thermal inertia nor the MEP-modeled ground heat flux contains obvious biases. The above analysis highlights the important role of ground heat flux data in the applications of the MEP model in these high-latitude regions. We also point out that there are inherent uncertainties associated with existing observations, possibly responsible for the noted phase shifts between the MEP-modeled results and observations, and propose a unified strategy for making ground heat flux measurements (Appendix E).

4. Indirect Validation of the MEP Model Using Sap Flow Measurements

At the Polar Urals site, subdaily sap flow data (raw voltage signals) are available from June to August in 2015 and 2016. Figure 7a shows that the daytime sap flow signals are consistent with the MEP-modeled daytime latent heat flux (MEP *E*). Changes in sap flow velocity are relatively smooth in time, as compared to the MEP *E*. However, both are responsive to large changes in net radiation, as exemplified in Figure 7a during midday on 18 July 2015 and 13 July 2016. Figure 7b illustrates the diurnal cycles of sap flow velocity (proxy), net radiation, and MEP *E* averaged over the analysis periods of summers of 2015 and 2016. It is of interest to note that there is a 1- to 2-hr lag between the diurnal peaks of sap flow signals and the peaks of net radiation and MEP *E*. During the evening, when net radiation and *E* diminish, the sap flow signals indicate a continued flow. This lagged sap flow may be indicative of evening-time transport and subsequent storage of water in the tree canopy or high “leakage” conductance of larch canopies. It would be possible to separate MEP *E* into soil evaporation and transpiration during the daytime, and to quantify water uptake (nontranspiring) during the nighttime, once the sap flow signals are converted to water flux and appropriately scaled based on canopy cover in the footprint of radiative flux measurements, but such an analysis is beyond the scope of this study.

5. The MEP Versus PM/P-M Model of PET

The purpose of testing the MEP PET model using two input variables (net radiation and surface temperature) is to confirm its capability to reproduce estimates with the widely accepted PM or P-M model that uses at least five input variables (net radiation, ground heat flux, air temperature, air humidity, and wind speed) and parameters including surface resistance, whose parameterization requires additional variables (Jarvis, 1976). Figure 8 compares the P-M PET and MEP PET models using half-hourly meteorological data at two selected sites, Imnavait Creek Ridge, AK and Vorkuta, Russia (Table 1). The close agreement between the P-M and MEP PET models justifies the MEP PET model as an advantageous alternative to the classical PET models that require multiple hydrometeorological data, often unavailable for Arctic regions. Figure 8 also shows a comparison of daily P-M versus MEP PET where the daily meteorological data are aggregated from the half-hourly data. The correlation between the daily P-M and MEP PET is even higher than that at subdaily time scale, with minor biases at higher PET.

6. Conclusions

This study analyzed surface energy budgets of the growing season at multiple sites in the Arctic region underlain by the permafrost. The sites are within a narrow band of 67–70°N latitude, and majority of them have eddy-covariance data of latent and sensible fluxes as well as ground heat fluxes. During the peak of the growing season, the surface energy budgets have similar features: Latent and sensible heat fluxes are nearly equal, with diurnal peaks around 200 W/m^2 and ground heat flux peaks around 50 W/m^2. Ground heat flux during July is net positive, implying surface heat source that leads to the development of seasonal active layer. The thermal inertia of the top soil layer covered with tundra vegetation is on the order of 400 tiu, substantially lower than that of common mineral soils in other regions.

The MEP PET model performance is similar to that of the classical P-M PET formulation over the studied sites in the Arctic. The MEP PET model uses only net radiation and surface temperature data and therefore is an advantageous PET model for data-sparse regions such as the Arctic.

Appendix A: Parameterization of I_0

The "apparent thermal inertia of the air" I_0 in equation (1) is formulated based on the Monin-Obukhov similarity equations (Wang & Bras, 2009):

$$I_0 = C_0 \rho c_p \sqrt{\kappa z} \left(\frac{\kappa z g}{\rho c_p T_0} \right)^{\frac{1}{6}} \tag{A1}$$

where$\rho$is the density of air (kg/m^3), c_p (1,004 J·kg^{-1}·K^{-1}) the specific heat of air at constant pressure,κ (~0.4) the von Karman constant, z the distance from the surface (m), g (9.8 m/s^2) is the gravitational acceleration, T_0 (~300 K) is the representative environment temperature, and

$$C_0 = \begin{cases} \left(\frac{\sqrt{3}}{\alpha} \right)^{\frac{1}{2}} \left(\frac{\gamma_2}{2} \right)^{\frac{1}{6}} \sim 1.7, & \text{unstable} \\ \left(\frac{2}{1+2\alpha} \right)^{\frac{1}{2}} (2\beta)^{\frac{1}{6}} \sim 1.2, & \text{stable} \end{cases} \tag{A2}$$

where α (~1), β (~4.6), and γ_2 (~9) are the coefficients in the empirical functions in the Monin-Obukhov similarity equations representing the effect of stability on mean wind shear and (potential) temperature gradient within the surface layer (Businger et al., 1971).

$$\sigma(T_s, q_s) = \frac{\lambda^2 q_s}{c_p R_v T_s^2} \tag{A3}$$

Equation (A3) defines σ, a dimensionless parameter that characterizes the phase-change-related state of the evaporating surface (Wang & Bras, 2011). The physical parameters in σ in equation (1) include the latent heat of vaporization of liquid water λ (2.5×10^6 J/kg), surface specific humidity q_s, surface temperature T_s in kelvin, and the gas constant of water vapor R_v (461 J·kg^{-1}·K^{-1}).

Appendix B: The Formula of the MEP Model for Snow (Water) Surfaces

The formulation of the MEP model of E, H, and water/snow surface heat flux Q over water/snow surfaces (Wang et al., 2014) is similar to that for land surface as in equation (1):

$$\begin{aligned} &E + H + Q = R_n^L \\ &E = B(\sigma)H \\ &Q = \frac{B(\sigma)}{\sigma}\frac{I_s}{I_0}H|H|^{-\frac{1}{6}} - R_n^s \end{aligned} \tag{B1}$$

where I_s is the thermal inertia of liquid water or snow and R_n^s and R_n^L are the surface net solar and longwave radiation fluxes, respectively, defined to be positive toward snow/water surfaces. The differences between equations (B1) and (1) are due to the fact that water and snow are transparent to sunlight, while soils are not. Note that q_s for the case of water/snow surface is a function of T_s according to the Clausius-Clapeyron equation since water vapor right above water/snow surface is assumed to be saturated at surface temperature:

$$q_s = \varepsilon \frac{e^*(T_s)}{P} = \varepsilon \frac{e_0}{P} \exp\left[\frac{\lambda_s}{R_v}\left(\frac{1}{T_0} - \frac{1}{T_s}\right)\right] \tag{B2}$$

where ε (= 0.62) is the ratio of molecular weight of water vapor to that of dry air, P the atmospheric pressure, e^*saturation vapor pressure, e_0 saturation vapor pressure at temperature T_0, and λ_s the latent heat of vaporization (2.5×10^6 J/kg) or sublimation (2.83×10^6 J/kg). Therefore, the model only needs data onR_n^s, R_n^L, and T_s. Note that the calculation of E and H only requires R_n and T_s data, according to equations (B1) and (B2).

Appendix C: Estimation of Soil Thermal Inertia I_s

The thermal inertia of a material surface, a required input to the MEP model, is defined as (Putzig, 2006)

$$I_s = \sqrt{k\rho c_h} \quad \left(\mathrm{tiu} \equiv \mathrm{J \cdot m^{-2} \cdot K^{-1} \cdot s^{-1/2}}\right) \tag{C1}$$

where k is the thermal conductivity (W·m^{-1}·K^{-1}), ρ the density (kg/m^3), and c_h the specific heat (J·kg^{-1}·K^{-1}) of the surface material. The soil material properties such as ρ, k, and c_h can be obtained from laboratory measurements. The specific heat, c_h, can be calculated as $c_h = \rho c_v$, where c_v is the soil volumetric heat capacity (J·m^{-3}·K^{-1}),

$$c_v = \theta_O c_{v,O} + \theta_I c_{v,I} + \theta_S c_{v,S} + \theta_A c_{v,A} \tag{C2}$$

where $c_{v,n}$ are the heat capacities with subscript n referring to soil organic "O," ice "I," solid "S," and air "A" components and θ_n their corresponding volumetric contents.

Several nonlinear mixing laws have been proposed to obtain the soil thermal conductivity (Fröb, 2011). Westermann et al. (2009) developed a method to directly calculate the thermal diffusivity of a soil column that can be used to estimate the soil thermal conductivity in combination with heat capacity. The thermal diffusivity d_h follows the one-dimensional heat transfer equation assuming constant specific heat and thermal conductivity:

$$\frac{\partial}{\partial t} T(z,t) = d_h \frac{\partial^2}{\partial z^2} T(z,t) \tag{C3}$$

with

$$d_h = \frac{k}{c_h} \tag{C4}$$

Time series of temperature of three different depths in a profile $T(z_{1,2,3},t)$ are required to derive d_h. The model of de Vries (1975) introduces an experimentally determined weighting factor to describe the impact

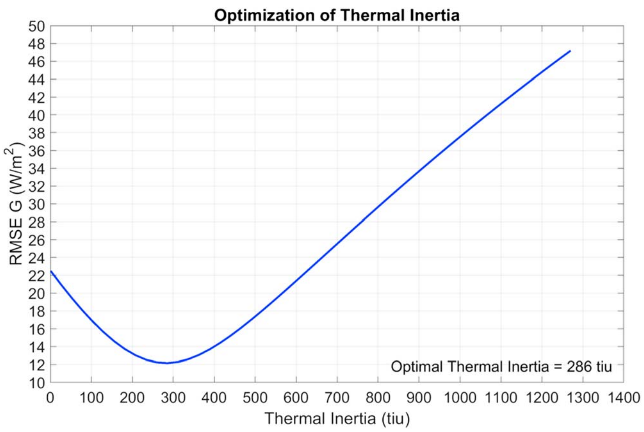

Figure C1. Estimate of surface thermal inertia I_s for the Tussock Flux Tower site at Imnavait Creek, AK, USA. RMSE = root mean square error.

of each soil component fraction. The modeling theory of Johansen (1975) proposed an approach based on soil grain size distribution combined with soil organic content. Further, the method performed by Endrizzi et al. (2011) uses a quadratic parallel mixing law (Cosenza et al., 2003) to calculate the soil thermal conductivity, which can be easily applied to frozen soils.

For reference, typical thermal inertia values of mineral soils are around 800–1,000 tiu (e.g., Nearing et al., 2012; Wang et al., 2010). Thermal inertia of still, pure liquid water is 1,560 tiu. Thermal inertia of snowpack varies with bulk density and thermal conductivity of snow (DeWalle & Rango, 2008). Vegetation or peat layer at the top of the soil is expected to have much lower thermal inertia than what can be obtained for mineral soils. When the thermal properties of the peat layer, the soil organic matter content, and spatial variability characteristics are unknown, the surface thermal inertia may be estimated as a fitting parameter of (MEP-) modeled versus observed ground heat fluxes.

Specifically, in this study, measured ground heat flux is used for the estimation of surface thermal inertia. It is obtained by minimizing the half-hourly RMSE between the MEP-modeled and in situ measured ground heat flux. Figure C1 illustrates I_s estimated based on the RMSE minimization for the Tussock Flux Tower site at Imnavait Creek, AK. I_s corresponding to the minimum RMSE is ~286 tiu, which is in the range of 200–400 tiu. Table A1 lists summer season surface thermal inertia for all study sites estimated using this approach. The obtained thermal inertia values are consistent with those of the moss-grass-air layer consisting of organic matter with 50–70% porosity reported previously (Campbell & Norman, 1998; de Vries, 1963).

Appendix D: P-M Equation

The PM and P-M models (Monteith, 1965) are two common models of PET using hydrometeorological data. In this study, PM or P-M PET is defined as the reference evapotranspiration of a well-watered grass crop adopted by the Food and Agriculture Organization of the United Nations (Allen et al., 1998) where the P-M equation is expressed as

$$\mathrm{PET} = \frac{\Delta(R_\mathrm{n} - G) + \rho c_\mathrm{p}(e_\mathrm{s} - e_\mathrm{a}) r_\mathrm{a}}{\Delta + \gamma(1 + r_\mathrm{s}/r_\mathrm{a})} \tag{D1}$$

$$r_\mathrm{s} = 70$$

$$r_\mathrm{a} = \frac{208}{u}$$

where R_n is net radiation, G ground heat flux, ρ the air density, c_p the specific heat of air (at constant pressure), e_s the saturated surface vapor pressure at air temperature, e_a the air vapor pressure, Δ the slope of vapor pressure curve, γ the psychrometric constant, r_s the (constant) surface resistance, and r_a the aerodynamic resistance in terms of wind speed u.

Table A1
Estimated Surface Thermal Inertia I_s (tiu) for the Five Study Sites Across the Arctic Region

Site name	Surface thermal inertia, I_s (tiu)
Ivotuk, AK, USA	234
Kuparuk River, AK, USA	411
Imnavait Creek: Ridge Flux Tower, AK, USA	441
Imnavait Creek: Tussock Flux Tower, AK, USA	286
Vorkuta, Russia	441
Polar Urals, Russia[a]	400

Note. A reference value of 400 tiu was assumed. tiu = thermal inertia unit.
[a]Monitoring site with no ground heat flux data.

Appendix E: Ground Heat Flux Measurements

Given the importance of ground heat flux for seasonal thaw dynamics and therefore the long-term fate of the permafrost, it is vital to accurately measure this flux properly. There are, however, inherent uncertainties associated with existing observations. Specifically, a typical heat flux sensor is a plate that measures temperature difference between the top and bottom faces generating voltage that can be calibrated to represent conductive heat transmission in the soil medium. Manuals for installation of heat flux plates instruct their placement 5–10 cm "below the surface," requiring full contact with the soil and absence of air pockets trapped near the plate; that is, the medium must be representative of the surrounding soil and avoid accumulation of water/ice on top of the plate. A

Figure E1. An example of installation of heat flux plate at the depth of 6 cm (cyan arrow) below the top of mineral soil in the Polar Urals, Russia. (a) The thickness of the "O" horizon and peat layer (yellow arrow) containing undecomposed and partially decomposed organics is ~6 cm. (b) For a different site with the same instrumentation setup, the peat thickness is ~12 cm, also containing a surface moss layer. Soil temperature sensors at the depths of 2 and 4 cm (black cables) as well as averaging soil moisture and temperature sensor at the same depth range (white plastic head) can be seen to the right of the heat flux plate in (a).

reconstruction of heat flux at the soil-air interface is then carried out by using auxiliary soil temperature gradient and moisture data in the layer above the heat flux plate (e.g., Campbell Scientific, 2016). However, the presence of peat mat and soil organic matter at the top of mineral soil (Figure E1), which are common in the Arctic regions due to low decomposition rates, can make an interpretation of these recommendations subjective: 5- to 10-cm depth can be considered with respect to the top of the layer containing partially decomposed peat layer/organic debris (the "O" soil horizon) or with respect to the top of mineral soil. As the peat layer has substantial spatial variability of thickness and properties (and, in fact, is not suitable for equipment installation due to inhomogeneity and presence of air voids), we posit that heat flux plates need to be installed at a fixed depth below the top of mineral soil (as an example, at 6 cm in Figure E1) and the heat flux is reconstructed for the soil-air boundary using traditional approaches (e.g., Campbell Scientific, 2016) that require auxiliary observations on temperature and wetness of both mineral soil and the peat layer.

Acknowledgments
This research is sponsored by the National Science Foundation Office of Polar Programs Grants 1725654 (University of Michigan), 1724868 (Kansas State University), and 1724633 (Georgia Tech). V. Ivanov and V. Mazepa acknowledge the support from project RUB1-7032-EK-11 funded by the U.S. Civilian Research and Development Foundation. V. Mazepa acknowledges the partial support from Grant RFBR-19-05-00756 from the Russian Foundation for Basic Research. Data used in this study are publicly accessible from the sources listed in Table 1. The eddy covariance flux data used in this study are provided by the FLUXNET community with data processing and harmonization carried out by the European Fluxes Database Cluster, AmeriFlux Management Project, and Fluxdata project of FLUXNET. AmeriFlux network was funded by the U.S. Department of Energy's Office of Science.

References

ACIA (2004). *Impacts of a warming Arctic: Arctic climate impact assessment*. ACIA Overview report (p. 140). Cambridge: Cambridge University Press.

Allen, R. G., Pereiro, L. S., Raes, D., & Smith, M. (1998). *Crop evapotranspiration: Guidelines for computing crop requirements*. Irrigation and Drainage paper No. 56. Rome: Food and Agriculture Organization (FAO).

Arya, S. P. (1988). *Introduction to micrometeorology* (pp. 123–140). Academic Press.

Auble, D. L., & Meyers, T. P. (1992). An open path, fast response infrared absorption gas analyzer for H_2O and CO_2. *Boundary-Layer Meteorol*, *59*(3), 243–256. https://doi.org/10.1007/BF00119815

Baldocchi, D., Falge, E., Gu, L., Olson, R., Hollinger, D., Running, S., et al. (2001). FLUXNET: A new tool to study the temporal and spatial variability of ecosystem-scale carbon dioxide, water vapor, and energy flux densities. *Bulletin of the American Meteorological Society*, *82*(11), 2415–2434. https://doi.org/10.1175/1520-0477(2001)082<2415:FANTTS>2.3.CO;2

Bekryaev, R. V., Polyakov, I. V., & Alexeev, V. A. (2010). Role of polar amplification in long-term surface air temperature variations and modern Arctic warming. *Journal of Climate*, *23*(14), 3888–3906. https://doi.org/10.1175/2010JCLI3297.1

Beringer, J., Chapin, F. S., Thompson, C. C., & McGuire, A. D. (2005). Surface energy exchanges along a tundra-forest transition and feedbacks to climate. *Agricultural and Forest Meteorology*, *131*(3-4), 143–161. https://doi.org/10.1016/j.agrformet.2005.05.006

Bhatt, U. S., Walker, D. A., Raynolds, M. K., Bieniek, P. A., Epstein, H. E., Comiso, J. C., et al. (2013). Recent declines in warming and vegetation greening trends over pan-Arctic tundra. *Remote Sensing*, *5*(9), 4229–4254. https://doi.org/10.3390/rs5094229

Boike, J. (2003). Seasonal snow cover on frozen ground: Energy balance calculations of a permafrost site near Ny-Ålesund, Spitsbergen. *Journal of Geophysical Research*, *108*(D2), 8163. https://doi.org/10.1029/2001JD000939

Bonfils, C., Phillips, T., Lawrence, D., Cameron-Smith, P., Riley, W., & Subin, M. (2012). On the influence of shrub height and expansion on northern high latitude climate. *Environmental Research Letters*, *7*, 15,503.

Brutsaert, W. (1982). *Evaporation into the atmosphere* (p. 216). Netherlands: Springer.

Businger, J. A., Wyngaard, J. C., Izumi, Y., & Bradley, E. F. (1971). Flux-profile relationships in the atmospheric surface layer. *Journal of the Atmospheric Sciences*, *28*(2), 181–189. https://doi.org/10.1175/1520-0469(1971)028<0181:FPRITA>2.0.CO;2

Campbell, G. S., & Norman, J. M. (1998). *An introduction to environmental biophysics* (p. 118). New York: Springer.

Chapin, F. S., Sturm, M., Serreze, M. C., McFadden, J. P., Key, J. R., Lloyd, A. H., et al. (2005). Role of land-surface changes in Arctic summer warming. *Science*, *310*(5748), 657–660. https://doi.org/10.1126/science.1117368

Cosenza, P., Guerin, R., & Tabbagh, A. (2003). Relationship between thermal conductivity and water content of soils using numerical modelling. *European Journal of Soil Science*, *54*(3), 581–588. https://doi.org/10.1046/j.1365-2389.2003.00539.x

Cristóbal, J., Prakash, A., Anderson, M. C., Kustas, W. P., Euskirchen, E. S., & Kane, D. L. (2017). Estimation of surface energy fluxes in the Arctic tundra using the remote sensing thermal-based Two-Source Energy Balance model. *Hydrology and Earth System Sciences*, *21*(3), 1339–1358. https://doi.org/10.5194/hess-21-1339-2017

Devi, N., Hagedorn, F., Moiseev, P., Bugmann, H., Shiyatov, S., Mazepa, V., & Rigling, A. (2008). Expanding forests and changing growth forms of Siberian larch at the Polar Urals treeline during the 20th century. *Global Change Biology*, *14*(7), 1581–1591. https://doi.org/10.1111/j.1365-2486.2008.01583.x

DeWalle, D. R., & Rango, A. (2008). *Principles of snow hydrology* (p. 61). Cambridge University Press.

Dewar, R. (2005). Maximum entropy production and the fluctuation theorem. *Journal of Physics A: Mathematical and General*, *38*, L371.

Dewar, R., Lineweaver, C., Niven, R., & Regenauer-Lieb, K. (2014). *Beyond the second law: Entropy production and non-equilibrium systems*. Springer.

Endrizzi, S., Quinton, W. L., & Marsh, P. (2011). Modelling the spatial pattern of ground thaw in a small basin in the arctic tundra. *The Cryosphere Discussions*, *5*(1), 367–400. https://doi.org/10.5194/tcd-5-367-2011

Eshonkulov, R., Poyda, A., Ingwersen, J., Pulatov, A., & Streck, T. (2019). Improving the energy balance closure over a winter wheat field by accounting for minor storage terms. *Agricultural and Forest Meteorology*, *264*, 283–296. https://doi.org/10.1016/j.agrformet.2018.10.012

Essery, R., & Pomeroy, J. (2004). Vegetation and topographic control of wind-blown snow distributions in distributed and aggregated simulations for an Arctic tundra basin. *Journal of Hydrometeorology*, *5*(5), 735–744. https://doi.org/10.1175/1525-7541(2004)005<0735:VATCOW>2.0.CO;2

Euskirchen, E. S., Bret-Harte, M. S., Scott, G. J., Edgar, C., & Shaver, G. R. (2012). Seasonal patterns of carbon dioxide and water fluxes in three representative tundra ecosystems in northern Alaska. *Ecosphere*, *3*.

Evett, S. R., Agam, N., Kustas, W. P., Colaizzi, P. D., & Schwartz, R. C. (2012). Soil profile method for soil thermal diffusivity, conductivity and heat flux: Comparison to soil heat flux plates. *Advances in Water Resources*, *50*, 41–54. https://doi.org/10.1016/j.advwatres.2012.04.012

Falge, E., M. Aubinet, Bakwin, P. S., Baldocchi, D., Berbigier, P., Bernhofer, C., et al. (2016). FLUXNET research network site characteristics, investigators, and bibliography. Oak Ridge National Laboratory (ORNL) DAAC, Tennessee, USA. https://doi.org/10.3334/ORNLDAAC/1530

Foken, T. (2008). The energy balance closure problem: An overview. *Ecological Applications*, *18*(6), 1351–1367. https://doi.org/10.1890/06-0922.1

Foley, J. A. (2005). Tipping points in the tundra. *Science*, *310*(5748), 627–628. https://doi.org/10.1126/science.1120104

Forbes, B. C., Fauria, M. M., & Zetterberg, P. (2010). Russian Arctic warming and 'greening' are closely tracked by tundra shrub willows. *Global Change Biology*, *16*(5), 1542–1554. https://doi.org/10.1111/j.1365-2486.2009.02047.x

Friborg, T., Biasi, C., & Shurpali, N. J. (2008). FLUXNET2015 RU-Vrk Seida/Vorkuta. https://doi.org/10.18140/FLX/1440245

Fröb, K. (2011). Measuring and modeling of soil thermal properties and ground heat flux at two different sites at Lena Delta, Siberia. Diplom thesis, University of Leipzig. Retrieved from http://epic.awi.de/25314/

Fuchs, M., & Tanner, C. B. (1968). Calibration and field test of soil heat flux plates. *Soil Science Society of America Journal*, *32*(3), 326–328. https://doi.org/10.2136/sssaj1968.03615995003200030021x

Gelaro, R., McCarty, W., Suárez, M. J., Todling, R., Molod, A., Takacs, L., et al. (2017). The Modern-Era Retrospective Analysis for Research and Applications, version 2 (MERRA-2). *Journal of Climate*, *30*(14), 5419–5454. https://doi.org/10.1175/JCLI-D-16-0758.1

Global Modeling and Assimilation Office (2015a). M2I1NXLFO: MERRA-2 inst1_2d_lfo_Nx: 2d, 1-hourly, instantaneous, single-level, assimilation, land surface forcings V5.12.4, Greenbelt, MD, USA, Goddard Earth Sciences Data and Information Services Center (GES DISC), Accessed: [Retrieved June 1, 2019], 10.5067/RCMZA6TL70BG.

Global Modeling and Assimilation Office (2015b). M2T1NXLND: MERRA-2 tavg1_2d_lnd_Nx: 2d,1-hourly, time-averaged, single-level, assimilation, land surface diagnostics V5.12.4, Greenbelt, MD, USA, Goddard Earth Sciences Data and Information Services Center (GES DISC), Accessed: [Retrieved June 1, 2019], 10.5067/RKPHT8KC1Y1T.

Granier, A. (1987). Sap flow measurements in Douglas-fir tree trunks by means of a new thermal method. *Annals of Forest Science*, *44*(1), 1–14. https://doi.org/10.1051/forest:19870101

Graversen, R. G., & Wang, M. (2009). Polar amplification in a coupled climate model with locked albedo. *Climate Dynamics*, *33*(5), 629–643. https://doi.org/10.1007/s00382-009-0535-6

Hajji, I., Nadeau, D. F., Music, B., Anctil, F., & Wang, J. (2018). Application of the maximum entropy production model of evapotranspiration over partially vegetated water-limited land surfaces. *Journal of Hydrometeorology*, *19*(6), 989–1005. https://doi.org/10.1175/JHM-D-17-0133.1

Hamman, J., Nijssen, B., Brunke, M., Cassano, J., Craig, A., DuVivier, A., et al. (2016). Land surface climate in the regional Arctic system model. *Journal of Climate*, *29*(18), 6543–6562. https://doi.org/10.1175/JCLI-D-15-0415.1

Heikkinen, J. E. P., Virtanen, T., Huttunen, J. T., Elsakov, V., & Martikainen, P. J. (2004). Carbon balance in East European tundra. *Global Biogeochemical Cycles*, *18*, GB1023. https://doi.org/10.1029/2003GB002054

Hinzman, L. D., Bettez, N. D., Bolton, W. R., Chapin, F. S., Dyurgerov, M. B., Fastie, C. L., et al. (2005). Evidence and implications of recent climate change in Northern Alaska and other Arctic regions. *Climatic Change*, *72*(3), 251–298. https://doi.org/10.1007/s10584-005-5352-2

Huang, S. Y., & Wang, J. (2016). A coupled force-restore model of surface temperature and soil moisture using the maximum entropy production model of heat fluxes. *Journal of Geophysical Research: Atmospheres*, *121*, 7528–7547. https://doi.org/10.1002/2015JD024586

Jarvis, P. G. (1976). The interpretation of the variations in leaf water potential and stomatal conductance found in canopies in the field. *Philosophical Transactions of the Royal Society of London. B, Biological Sciences*, *273*(927), 593–610. https://doi.org/10.1098/rstb.1976.0035

Jaynes, E. T. (1957). Information theory and statistical mechanics. *Physical Review*, *106*(4), 620–630. https://doi.org/10.1103/PhysRev.106.620

Jaynes, E. T., & Bretthorst, G. L. (2003). *Probability theory—The logic of science*. Cambridge University Press.

Jeong, J.-H., Kug, J. S., Kim, B. M., Min, S.-K., Linderholm, H., Ho, C.-H., et al. (2012). Greening in the circumpolar high-latitude may amplify warming in the growing season. *Climate Dynamics*, *38*, 1421–1431.

Jia, G. J., Epstein, H. E., & Walker, D. A. (2003). Greening of arctic Alaska, 1981–2001. *Geophysical Research Letters*, *30*(20), 2067. https://doi.org/10.1029/2003GL018268

Jia, G. J., Epstein, H. E., & Walker, D. A. (2009). Vegetation greening in the Canadian Arctic related to decadal warming. *Journal of Environmental Monitoring*, *11*(12), 2231–2238. https://doi.org/10.1039/b911677j

Johansen, O. (1975). *Thermal conductivity of soils* (p. 236). University of Trondheim.

Juretić, D., & Županović, P. (2003). Photosynthetic models with maximum entropy production in irreversible charge transfer steps. *Computational Biology and Chemistry*, *27*(6), 541–553. https://doi.org/10.1016/j.compbiolchem.2003.09.001

Kapur, J. N. (1989). *Maximum-entropy models in science and engineering*. John Wiley and Sons.

Kleidon, A., & Fraedrich, K. (2006). *14 biotic entropy production and global atmosphere-biosphere interactions* (pp. 173–189). Springer-Verlag.

Kleidon, A., & Lorenz, R. D. (2005). *Non-equilibrium thermodynamics and the production of entropy*. Springer-Verlag. https://doi.org/10.1007/b12042

Kleidon, A., Malhi, Y., & Cox, P. M. (2010). Maximum entropy production in environmental and ecological systems. *Philosophical Transactions of the Royal Society of London. Series B, Biological sciences*, *365*(1545), 1297–1302. https://doi.org/10.1098/rstb.2010.0018

Kleidon, A., & Schymanski, S. (2008). Thermodynamics and optimality of the water budget on land: A review. *Geophysical Research Letters*, *35*, L20404. https://doi.org/10.1029/2008GL035393

Laskowski, C. (2010). Spatial and temporal patterns of carbon exchange in the Alaskan Arctic tundra ecosystem. (PhD dissertation in Ecology). University of California Davis and San Diego State University.

Lee, Y.-H., & Mahrt, L. (2004). An evaluation of snowmelt and sublimation over short vegetation in land surface modelling. *Hydrological Processes*, *18*(18), 3543–3557. https://doi.org/10.1002/hyp.5799

Liston, G. E., McFadden, J. P., Sturm, M., & Pielke, R. A. (2002). Modelled changes in arctic tundra snow, energy and moisture fluxes due to increased shrubs. *Global Change Biology*, *8*(1), 17–32. https://doi.org/10.1046/j.1354-1013.2001.00416.x

Lloyd, C. R., Harding, R. J., Friborg, T., & Aurela, M. (2001). Surface fluxes of heat and water vapour from sites in the European Arctic. *Theoretical and Applied Climatology*, *70*(1-4), 19–33. https://doi.org/10.1007/s007040170003

Loranty, M. M., Abbott, B. W., Blok, D., Douglas, T. A., Epstein, H. E., Forbes, B. C., et al. (2018). Reviews and syntheses: Changing ecosystem influences on soil thermal regimes in northern high-latitude permafrost regions. *Biogeosciences*, *15*(17), 5287–5313. https://doi.org/10.5194/bg-15-5287-2018

Loranty, M. M., & Goetz, S. J. (2012). Shrub expansion and climate feedbacks in Arctic tundra. *Environmental Research Letters*, *7*(1). https://doi.org/10.1088/1748-9326/7/1/011005

Loranty, M. M., Lieberman-Cribbin, W., Berner, L. T., Natali, S. M., Goetz, S. J., Alexander, H. D., & Kholodov, A. L. (2016). Spatial variation in vegetation productivity trends, fire disturbance, and soil carbon across arctic-boreal permafrost ecosystems. *Environmental Research Letters*, *11*(9). https://doi.org/10.1088/1748-9326/11/9/095008

Lund, M., Hansen, B. U., Pedersen, S. H., Stiegler, C., & Tamstorf, M. P. (2014). Characteristics of summer-time energy exchange in a high Arctic tundra heath 2000–2010. *Tellus B: Chemical and Physical Meteorology*, *66*.

Lund, M., Stiegler, C., Abermann, J., Citterio, M., Hansen, B. U., & van As, D. (2017). Spatiotemporal variability in surface energy balance across tundra, snow and ice in Greenland. *Ambio*, *46*(S1), 81–93. https://doi.org/10.1007/s13280-016-0867-5

Mazepa, V., Ivanov, V., Shiyatov, S., & Sheshukov, A. Y. (2019). Surface energy budgets in the Polar Urals of Russia in summer 2015–2017. Arctic Data Center. https://doi.org/10.18739/A2C824D80

Mazepa, V. S. (2005). Stand density in the last millennium at the upper tree-line ecotone in the Polar Ural Mountains. *Canadian Journal of Forest Research*, *35*(9), 2082–2091. https://doi.org/10.1139/x05-111

Monteith, J. L. (1965). Evaporation and environment. *Symposia of the Society for Experimental Biology*, *205-234*.

Nearing, G. S., Moran, M. S., Scott, R. L., & Ponce-Campos, G. (2012). Coupling diffusion and maximum entropy models to estimate thermal inertia. *Remote Sensing of Environment*, *119*, 222–231. https://doi.org/10.1016/j.rse.2011.12.012

Oechel, W. (1994). (US-Upa) Upad. AmeriFlux. [Available online at doi:10.17190/AMF/1246108.]

Oechel, W. C., Hastings, S. J., Vourlrtis, G., Jenkins, M., Riechers, G., & Grulke, N. (1993). Recent change of Arctic tundra ecosystems from a net carbon dioxide sink to a source. *Nature*, *361*(6412), 520–523. https://doi.org/10.1038/361520a0

Oncley, S. P., Foken, T., Vogt, R., Kohsiek, W., DeBruin, H. A. R., Bernhofer, C., et al. (2007). The Energy Balance Experiment EBEX-2000. Part I: Overview and energy balance. *Boundary-Layer Meteorology*, *123*(1), 1–28. https://doi.org/10.1007/s10546-007-9161-1

Osborne, E., Richter-Menge, J., & Jeffries, M. (Eds.) 2018: Arctic report card 2018. National Oceanic and Atmospheric Administration (NOAA) (114 pp.). https://www.arctic.noaa.gov/Report-Card

Osterkamp, T. E., & Romanovsky, V. E. (1999). Evidence for warming and thawing of discontinuous permafrost in Alaska. *Permafrost and Periglacial Processes*, *10*(1), 17–37. https://doi.org/10.1002/(SICI)1099-1530(199901/03)10:1<17::AID-PPP303>3.0.CO;2-4

Overpeck, J., Hughen, K., Hardy, D., Bradley, R., Case, R., Douglas, M., et al. (1997). Arctic environmental change of the last four centuries. *Science*, *278*(5341), 1251–1256. https://doi.org/10.1126/science.278.5341.1251

Parazoo, N. C., Arneth, A., Pugh, T. A. M., Smith, B., Steiner, N., Luus, K., et al. (2018). Spring photosynthetic onset and net CO_2 uptake in Alaska triggered by landscape thawing. *Global Change Biology*, *24*(8), 3416–3435. https://doi.org/10.1111/gcb.14283

Pomeroy, J. W., Bewley, D. S., Essery, R. L. H., Hedstrom, N. R., Link, T., Granger, R. J., et al. (2006). Shrub tundra snowmelt. *Hydrological Processes*, *20*(4), 923–941. https://doi.org/10.1002/hyp.6124

Pomeroy, J. W., Marsh, P., & Gray, D. M. (1997). Application of a distributed blowing snow model to the Arctic. *Hydrological Processes*, *11*(11), 1451–1464. https://doi.org/10.1002/(SICI)1099-1085(199709)11:11<1451::AID-HYP449>3.0.CO;2-Q

Pomeroy, J. W., Toth, B., Granger, R. J., Hedstrom, N. R., & Essery, R. L. H. (2003). Variation in surface energetics during snowmelt in a subarctic mountain catchment. *Journal of Hydrometeorology*, *4*(4), 702–719. https://doi.org/10.1175/1525-7541(2003)004<0702:VISEDS>2.0.CO;2

Post, E., Forchhammer, M. C., Bret-Harte, M. S., Callaghan, T. V., Christensen, T. R., Elberling, B., et al. (2009). Ecological dynamics across the Arctic associated with recent climate change. *Science*, *325*(5946), 1355–1358. https://doi.org/10.1126/science.1173113

Putzig, N. E. (2006). Thermal inertia and surface heterogeneity on Mars, Department of Geological Sciences, University of Colorado (195 pp.). Retrieved from http://nathaniel.putzig.com/research/dissertation/dissertation.pdf

Qiu, C., Zhu, D., Ciais, P., Guenet, B., Krinner, G., Peng, S., et al. (2018). ORCHIDEE-PEAT (revision 4596), a model for northern peatland CO_2, water, and energy fluxes on daily to annual scales. *Geoscientific Model Development*, *11*(2), 497–519. https://doi.org/10.5194/gmd-11-497-2018

Repo, M. E., Susiluoto, S., Lind, S. E., Jokinen, S., Elsakov, V., Biasi, C., et al. (2009). Large N_2O emissions from cryoturbated peat soil in tundra. *Nature Geoscience*, *2*(3), 189–192. https://doi.org/10.1038/ngeo434

Riedel, S. M., Epstein, H. E., Walker, D. A., Richardson, D. L., Calef, M. P., Edwards, E., & Moody, A. (2005). Spatial and temporal heterogeneity of vegetation properties among four tundra plant communities at Ivotuk, Alaska, U.S.A. *Arctic, Antarctic, and Alpine Research*, *37*(1), 25–33. https://doi.org/10.1657/1523-0430(2005)037[0025:SATHOV]2.0.CO;2

Sauer, T. J., & Horton, R. (2005). Soil Heat Flux Publications from USDA-ARS/UNL Faculty. 1402. http://digitalcommons.unl.edu/usdaarsfacpub/1402. Published in *Micrometeorology in Agricultural Systems* (2005) Agronomy Monograph no. 47: 131-154.

Schramm, I., Boike, J., Bolton, W. R., & Hinzman, L. D. (2007). Application of TopoFlow, a spatially distributed hydrological model, to the Imnavait Creek watershed, Alaska. *Journal of Geophysical Research*, *112*, G04S46. https://doi.org/10.1029/2006JG000326

Schuur, E. A. G., McGuire, A. D., Schädel, C., Grosse, G., Harden, J. W., Hayes, D. J., et al. (2015). Climate change and the permafrost carbon feedback. *Nature*, *520*(7546), 171–179. https://doi.org/10.1038/nature14338

Campbell Scientific (2016). Model HFP01 soil heat flux plate instruction manual. Revision 10/16. Campbell Scientific, Inc.

Screen, J. A., & Simmonds, I. (2010). The central role of diminishing sea ice in recent Arctic temperature amplification. *Nature*, *464*(7293), 1334–1337. https://doi.org/10.1038/nature09051

Serreze, M. C., Barrett, A., Stroeve, J. C., Kindig, D. N., & Holland, M. M. (2009). The emergence of surface-based Arctic amplification. *The Cryosphere*, *3*(1), 11–19. https://doi.org/10.5194/tc-3-11-2009

Serreze, M. C., & Francis, J. A. (2006). The Arctic amplification debate. *Climatic Change*, *76*(3-4), 241–264. https://doi.org/10.1007/s10584-005-9017-y

Serreze, M. C., Walsh, J. E., Chapin, F. S., Osterkamp, T., Dyurgerov, M., Romanovsky, V., et al. (2000). Observational evidence of recent change in the northern high-latitude environment. *Climatic Change*, *46*(1/2), 159–207. https://doi.org/10.1023/A:1005504031923

Shanafield, M., Cook, P. G., Gutiérrez-Jurado, H. A., Faux, R., Cleverly, J., & Eamus, D. (2015). Field comparison of methods for estimating groundwater discharge by evaporation and evapotranspiration in an arid-zone playa. *Journal of Hydrology*, *527*, 1073–1083. https://doi.org/10.1016/j.jhydrol.2015.06.003

Shipley, B. (2010). *From plant traits to vegetation structure: Chance and selection in the assembly of ecological communities*. Cambridge University Press.

Shiyatov, S. G., Terent'ev, M. M., & Fomin, V. V. (2005). Spatiotemporal dynamics of forest–tundra communities in the Polar Urals. *Russian Journal of Ecology*, *36*(2), 69–75. https://doi.org/10.1007/s11184-005-0051-9

Shiyatov, S. G., Terent'ev, M. M., Fomin, V. V., & Zimmermann, N. E. (2007). Altitudinal and horizontal shifts of the upper boundaries of open and closed forests in the Polar Urals in the 20th century. *Russian Journal of Ecology*, *38*(4), 223–227. https://doi.org/10.1134/S1067413607040017

Snyder, P. K. (2013). Arctic greening: Concerns over Arctic warming grow. *Nature Climate Change*, *3*(6), 539–540. https://doi.org/10.1038/nclimate1914

Soegaard, H., Hasholt, B., Friborg, T., & Nordstroem, C. (2001). Surface energy- and water balance in a high-arcticenvironment in NE Greenland. *Theoretical and Applied Climatology*, *70*(1-4), 35–51. https://doi.org/10.1007/s007040170004

Spielhagen, R. F., Werner, K., Sørensen, S. A., Zamelczyk, K., Kandiano, E., Budeus, G., et al. (2011). Enhanced modern heat transfer to the Arctic by warm Atlantic Water. *Science*, *331*(6016), 450–453. https://doi.org/10.1126/science.1197397

Sturm, M., Holmgren, J., McFadden, J. P., Liston, G. E., Chapin, F. S., & Racine, C. H. (2001). Snow–shrub interactions in Arctic tundra: A hypothesis with climatic implications. *Journal of Climate*, *14*(3), 336–344. https://doi.org/10.1175/1520-0442(2001)014<0336:SSIIAT>2.0.CO;2

Sturm, M., Schimel, J., Michaelson, G., Welker, J. M., Oberbauer, S. F., Liston, G. E., et al. (2005). Winter biological processes could help convert Arctic tundra to shrubland. *BioScience*, *55*(1), 17–26. https://doi.org/10.1641/0006-3568(2005)055[0017:WBPCHC]2.0.CO;2

Swann, A. L., Fung, I. Y., Levis, S., Bonan, G. B., & Doney, S. C. (2010). Changes in Arctic vegetation amplify high-latitude warming through the greenhouse effect. *Proceedings of the National Academy of Sciences*, *107*(4), 1295–1300. https://doi.org/10.1073/pnas.0913846107

Twine, T. E., Kustas, W. P., Norman, J. M., Cook, D. R., Houser, P. R., Meyers, T. P., et al. (2000). Correcting eddy-covariance flux underestimates over a grassland. *Agricultural and Forest Meteorology*, *103*(3), 279–300. https://doi.org/10.1016/S0168-1923(00)00123-4

Ueyama, M., Ichii, K., Iwata, H., Euskirchen, E. S., Zona, D., Rocha, A. V., et al. (2014). Change in surface energy balance in Alaska due to fire and spring warming, based on upscaling eddy covariance measurements. *Journal of Geophysical Research: Biogeosciences*, *119*, 1947–1969. https://doi.org/10.1002/2014JG002717

Vourlitis, G. L., & Oechel, W. C. (1997). Landscape-scale CO_2, H_2O vapour and energy flux of moist-wet coastal tundra ecosystems over two growing seasons. *Journal of Ecology*, *85*(5), 575–590. https://doi.org/10.2307/2960529

de Vries, D. A. (1963). In W. R. V. Wijk (Ed.), *Thermal properties of soils. Physics of Plant Environment* (pp. 210–235). John Wiley & Sons.

de Vries, D. A. (1975). In D. A. de Vries & N. F. Afgan (Eds.), *Heat transfer in soils. Heat and mass transfer in the biosphere. I. Transfer processes in plant environment* (pp. 5–28). Wiley.

Walker, D. A., & Acevedo, W. (1987). Vegetation and a Landsat-derived land cover map of the Beechey Point Quadrangle, Arctic Coastal Plain, Alaska. Cold Regions Research and Engineering Laboratory.

Wang, H., Tetzlaff, D., & Soulsby, C. (2017). Testing the maximum entropy production approach for estimating evapotranspiration from closed canopy shrubland in a low-energy humid environment. *Hydrological Processes*, *31*(25), 4613–4621. https://doi.org/10.1002/hyp.11363

Wang, J., & Bras, R. L. (2009). A model of surface heat fluxes based on the theory of maximum entropy production. *Water Resources Research*, *45*, W11422. https://doi.org/10.1029/2009WR007900

Wang, J., & Bras, R. L. (2011). A model of evapotranspiration based on the theory of maximum entropy production. *Water Resources Research*, *47*, W03521. https://doi.org/10.1029/2010WR009392

Wang, J., Bras, R. L., Nieves, V., & Deng, Y. (2014). A model of energy budgets over water, snow, and ice surfaces. *Journal of Geophysical Research: Atmospheres*, *119*, 6034–6051. https://doi.org/10.1002/2013JD021150

Wang, J., Bras, R. L., Sivandran, G., & Knox, R. G. (2010). A simple method for the estimation of thermal inertia. *Geophysical Research Letters*, *37*, L05404. https://doi.org/10.1029/2009GL041851

Westermann, S., Lüers, J., Langer, M., Piel, K., & Boike, J. (2009). The annual surface energy budget of a high-arctic permafrost site on Svalbard, Norway. *The Cryosphere*, *3*(2), 245–263. https://doi.org/10.5194/tc-3-245-2009

Wilson, K., Goldstein, A., Falge, E., Aubinet, M., Baldocchi, D., Berbigier, P., et al. (2002). Energy balance closure at FLUXNET sites. *Agricultural and Forest Meteorology*, *113*(1-4), 223–243. https://doi.org/10.1016/S0168-1923(02)00109-0

Xu, D., Agee, E., Wang, J., & Ivanov, V. Y. (2019). Estimation of evapotranspiration of Amazon rainforest using the maximum entropy production method. *Geophysical Research Letters*, *46*, 1402–1412. https://doi.org/10.1029/2018GL080907

10.1029/2019JD030650

Yang, J., & Wang, Z.-H. (2014). Land surface energy partitioning revisited: A novel approach based on single depth soil measurement. *Geophysical Research Letters*, *41*, 8348–8358. https://doi.org/10.1002/2014GL062041

Yi, Y., Kimball, J. S., Chen, R. H., Moghaddam, M., Reichle, R. H., Mishra, U., et al. (2018). Characterizing permafrost active layer dynamics and sensitivity to landscape spatial heterogeneity in Alaska. *The Cryosphere*, *12*(1), 145–161. https://doi.org/10.5194/tc-12-145-2018

Zona, D., & Oechel, W. (2004-2007). FLUXNET2015 US-Ivo Ivotuk. https://doi.org/10.18140/FLX/1440073